

Line shape study of acetylene transitions in the $\nu_1 + \nu_2 + \nu_4 + \nu_5$ band over a range of temperatures

Chad Povey^a, Adriana Predoi-Cross^{a,*}, Daniel R. Hurtmans^b

^a Department of Physics and Astronomy, University of Lethbridge, 4401 University Drive, Lethbridge, AB, Canada T1K 3M4

^b Service de Chimie Quantique et Photophysique CP 160/09, Université Libre de Bruxelles, 50, Av. Roosevelt, B-1050 Bruxelles, Belgium

ARTICLE INFO

Article history:

Available online 10 May 2011

Keywords:

Temperature variable cell
Spectroscopy
Absorption
Control software
Laser spectroscopy
Acetylene
Spectral line shapes

ABSTRACT

In this study we have retrieved the line intensities, self broadened widths, pressure-induced shifts and selected line mixing coefficients for 20 R-branch transitions in the $\nu_1 + \nu_2 + \nu_4 + \nu_5$ band of acetylene. The spectra were recorded using our 3-channels diode laser spectrometer, a temperature controlled cell of fixed length and a second, room temperature cell. The Voigt and speed-dependent Voigt profiles with inclusion of line mixing effects were used to retrieve the line parameters. We determined the temperature dependencies for line broadening, shift and line mixing coefficients.

© 2011 Elsevier Inc. All rights reserved.

1. Introduction

In the past decade numerous acetylene transitions have been used as frequency standards for fiber optic communications [1 and references therein]. Most of the spectroscopic studies are dedicated to the astrophysical and planetary applications of acetylene's line parameters. For example, spectra of Titan's atmosphere recorded by the Cassini instrument reported that acetylene is one of the most abundant trace constituents after methane [2].

The first study on record focused on measuring self- and H₂-broadened line parameters in acetylene is by Varanasi and Bangaru [3]. Laser spectroscopy was used by Wong [4] to measure the self-broadening coefficients for acetylene for transitions in the range of his dye laser. The self-broadening parameters of acetylene in the ν_5 band for 27 R and P-branch transitions were first studied by Lambot et al. [5] using a diode laser spectrometer. Pine [6] used a difference frequency laser system to measure the self-, N₂- and Ar-broadening coefficients for acetylene transitions in the $\nu_1 + \nu_5$ band. A follow-up study of Ref. [5] reports on the low temperature spectrum [7] of 21 transitions in the same band. Lucchesini et al. [8] used diode laser spectroscopy to measure self-broadening and shifting for several weak acetylene transitions belonging to overtone bands located in the 12 700 to 11 800 cm⁻¹ spectral range. Laser

spectroscopy was also used by Georges et al. [9] to measure Ar- and self-broadening in one transition of the 5 ν_3 band of acetylene.

Biswas et al. [10] have studied self- and nitrogen-broadening for transitions in the $\nu_1 + 3\nu_3$ band using spectra recorded with a diode laser spectrometer working nearby 782 cm⁻¹. Transitions in the same band were studied by Herregodts et al. [11] using a Ti:Sa autoscan laser spectrometer. Diode laser spectroscopy was used by Yelleswarapu and Sharma [12] to measure the self-broadening and pressure-induced self- shifts for several transitions in the $\nu_1 + 3\nu_3$ band. The spectra were modeled using the Voigt profile.

Minutolo et al. [13] measured self-, N₂-, O₂- and CO₂-broadening and pressure shifts for transitions of C₂H₂ and H¹³C¹²CH in four combination bands located in the 1.54 μ m range. Twenty acetylene transitions belonging to the $\nu_1 + 3\nu_3$ band have been studied in detail by Valipour and Zimmerman [14] with numerous broadeners: acetylene, N₂, O₂, air, He, Ne, Ar, Kr, Xe. An extensive study of cold bands located in the 5 μ m range was performed by Jacquemart et al. [15].

Thirty absorption lines in the $\nu_4 + \nu_5$ band of acetylene were recorded and studied by Lepere et al. [16].

Jacquemart et al. [17] measured line parameters for 550 lines belonging to 13 acetylene bands located between 1.7 and 1.9 μ m. Self-broadening coefficients have also been measured for 10 P branch transitions located nearby 1.533 μ m. Ten self-broadened P-branch transitions in the $\nu_1 + \nu_3$ band of acetylene have been studied by Li et al. [18] using diode laser spectroscopy.

In this study, using the 3-channels tunable diode laser spectrometer described in the following sections we have measured

* Corresponding author. Fax: +1 403 329 2057.

E-mail address: Adriana.predoiross@uleth.ca (A. Predoi-Cross).

20 lines in the $\nu_1 + \nu_2 + \nu_4 + \nu_5$ band of acetylene specifically examining the effects due to temperature and pressure changes. A selection of six pressures has been chosen and for each pressure seven temperatures were used ranging from 213 K to 350 K.

2. Experimental details

2.1. Background information on temperature controlled cells

We have developed a 3-channels tunable diode laser spectrometer that can be used to complete temperature and pressure controlled line shape studies on atmospheric gases. This research apparatus may be used for the spectroscopic characterization of molecules found within planetary atmospheres, by high-resolution laboratory studies.

For atmospheric research, long path lengths are required for absorption cells at various temperatures [19] and pressures. White type cells typically meet the prerequisite for path length due to their multi-pass configurations [20]. Ref. [21] reports on a long path cell (16–96 m) that operates between 215 and 470 K at gas pressures ranging from vacuum to 10 atm. A temperature controlled White type long path cell was built by McKellar [22,23] to enable studies of weakly bound complexes at low temperatures. The cell has a base of 5 m and allows the users to achieve up to 100 m pathlength. Another example of a variable temperature absorption cell (White design) that can accommodate path lengths up to 512 m and pressures up to 5 atm was built for laboratory spectroscopic studies of gases found in terrestrial and planetary atmospheres [24–28]. A large fraction of the published results are restricted to temperatures near room temperature. Ref. [29] provides a good example at the other end of the temperature range using the concept of collisional cooling within their cell. The minimum temperature that can be maintained in the cell is 10–12 K.

Over the last few decades many variable temperature cells have been published, but a key concern commonly examined within them is the temperature variability and instability of the cell. Short term stability is necessary for the efficient use of any cell as it reduces the time for experimental procedures within the laboratory. In 2004, Valentin et al. [30] reported on a stabilized low temperature infrared absorption cell cooled by an open cycle refrigerator, which can run with liquid nitrogen from 250 to 80 K or with liquid helium from 80 K to a few K. The authors have reported temperature stability better than 0.1 K within 4 h for a 300 to 4.5 K temperature spread. Other absorption cells reported within the literature deviate little from this range of temperatures and stability values.

Thermal gradients are often impossible to completely alleviate from the design of absorption cells but improvements have been made within this area. Multiple temperatures sensors are often used to monitor the temperature variability of the cells over their base length. Smith and colleagues [31] mounted six thermocouples in contact with their coolant along the length of their cell and have measured an agreement of ± 2 K between them. Eight thermocouples are distributed evenly along another cell built by Cann [32] and three were employed within Schaeffer et al.'s [33] multi-pass high temperature cell achieving accuracy of ± 1 K. Gradients less than 0.1 K/m have also been shown within Ref. [21]. The behavior of these thermal gradients is obvious and is highly dependent upon the base length of the cell. Accordingly, a compromise between a desired optical path length and thermal congruence is often necessary.

A 147.5 cm long variable-temperature absorption gas cell was designed [34] and built for spectroscopic measurements of gases of atmospheric interest using a Bomem DA8.3 Fourier transform

spectrometer. The heating/cooling system enveloping the cell allows spectroscopic studies of gas samples at temperatures ranging from 205 to 350 K and at pressures up to atmospheric pressure. The temperature gradients inside the cell are within ± 0.31 K, highlighting the very good performance of this system.

A short coolable gas cell designed for lineshape studies was presented by Lambot et al. [7]. The temperature can be stabilized to within 2 K for temperatures between 120 K and room temperature and accommodates any absorption pathlength between 0 and 3 cm. An experimental setup that integrates a low-temperature optical cell UV–visible (UV–Vis) with a liquid X-ray absorption spectroscopy (XAS) cell is reported in Ref. [35]. The proposed gas cell is suitable for the measurement of gases at variable temperatures from room temperature to 195 K.

2.2. Mechanical and optical design of the variable temperature cell

The overall design of the system is presented in Fig. 1. The first channel contains the temperature and pressure controlled cell. The second channel contains a room temperature reference cell of similar path length. The third channel records the background of the laser system. By measuring all three channels simultaneously we are able to perform accurate line shape analysis including pressure-induced line shift measurements.

The pathlength of the variable temperature cell presented here is 1.54 m. The 3-D layout of the temperature controlled cell is presented in Fig. 2. We have employed two main design features: (i) the absorption cell which is centered inside a vacuum jacket to minimize the thermal conductive/convective coupling to the outside cell and (ii) heating/cooling will be supplied by temperature-controlled fluid in direct contact with almost the complete cell body ensuring that the temperature gradients are minimized. The mechanical and optical components have been selected while paying attention to the type of gases (both stable and flammable) that will be studied.

The inner chamber is a single-pass cell and is made up of a nominal 4" schedule 40 stainless steel pipe that is 5' long. Both ends have a welded custom designed stainless steel flange which has four ports each where both flanges have the same diameter as the pipe. One of the flanges has two temperature ports, one pressure port, and a gas inlet port. The other flange has three temperature ports and one gas outlet port. Platinum resistor thermometers are mounted on rods and attached to the cell flanges by 1/8" diameter fittings. The 6", 18", and 30" long rods are mounted as shown in Fig. 2 to ensure that we are able to monitor the temperature at various depths of the cell with an additional sensor being mounted within the vacuum jacket.

The gas pressure inside the inner cell is measured using a MKS pressure module (0–1000 Torr) with a Model 670 signal conditioner which is monitored via LabVIEW software. The center counter-bore in the end flanges house crystal windows that can be interchanged for the desired spectral range. At the moment the cell is provided with anti-reflection coated CaF_2 windows. To suppress channel spectra caused by multiple reflections of the sample beam between the surfaces of the windows, the windows are also wedged. Fluoro-silicone O-rings are used on the inner sides of the crystal to seal the CaF_2 windows to the inner test chamber. The chamber is completely sealed from the outside. A stainless steel compression ring is applied to the outside side of each window to hold the window and o-ring assembly together.

The coolant fluid is supplied through a second chamber of 6" diameter shown in Fig. 2. This chamber is configured with six fins that allow the fluid to flow uniformly across the length of the cell. The heating/cooling of the gas inside the temperature controlled cell is provided by a Neslab ULT-80 thermal bath using ethanol or methanol as the coolant. The Neslab Chiller ULT-80 is needed

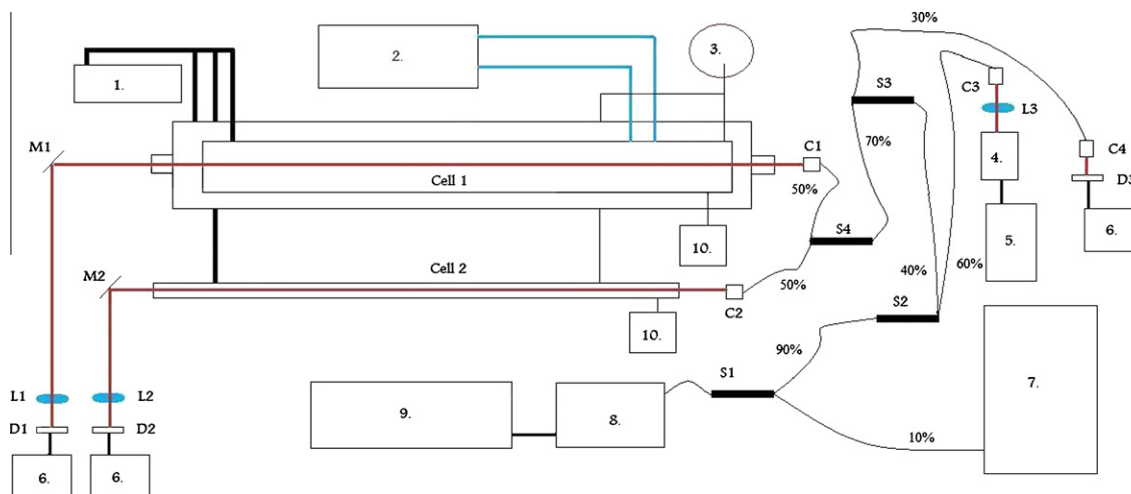


Fig. 1. General block diagram of current spectrometer setup. *Legend:* 1 – vacuum system; 2 – cooling system NesLab ULT 80 Chiller; 3 – gas sample; 4 and 5 – fabry Perot interferometer and controller; 6 – detector pre-amps and power supplies; 7 – WA-1500 EXFO wavemeter; 8 and 9 – velocity diode laser head and controller; 10 – MKS Baratron pressure gauges; L1, L2, L3 – focusing lenses; M1 and M2 – directing mirrors; D1, D2 and D3 – InGas detectors; C1–C4 – collimators; S1–S4 – fiber splitters; Vacuum lines are shown in thick black lines. Coolant lines are shown in blue. Laser path is shown by the red lines. Thin curved lines show fiber optic cables. (For interpretation of the references to color in this figure legend, the reader is referred to the web version of this article.)

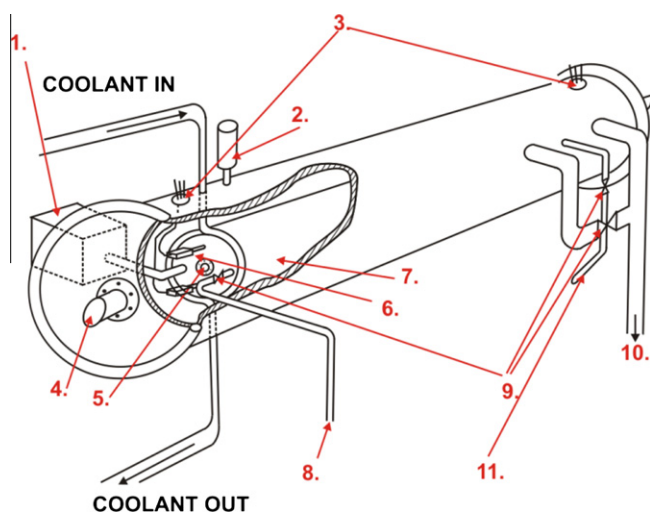


Fig. 2. Three-dimensional view of the temperature controlled gas cell. *Legend:* 1 – MKS Baratron pressure gauge, 2 – enhanced pirani pressure gauge, 3 – vacuum feed throughs, 4 – CaF₂ windows positioned at Brewster angle, 5 – CaF₂ windows for the inner cell, 6 – platinum resistor thermometers, 7 – inner cell body, 8 – gas inlet, 9 – vacuum valves, 10 – gas outlet, 11 – port for de-pressuring the vacuum jacket.

to vary the temperature of the gas between 193 and 353 K inside the temperature-controlled cell. The entire inner chamber rests on adjustable support stands to provide alignment of the inner chamber once placed inside the outer chamber.

The outer chamber is made up of nominal 8 in. schedule 10 stainless steel pipe that is 8" long. This larger chamber houses the inner chamber and is held under constant vacuum. Weld stubs have been specifically placed to allow points of entry for the temperature sensors, sample gas inlet and outlet, pressure monitoring lines, heated or cooled fluid inlet and outlet, and for pressure equalizing. Both ends of the outer chamber are removable to allow access to the inner chamber gas supply/outlet valves and thermocouples. The center of the end flanges has an interchangeable piece which houses an additional crystal and set at a desired angle. This outer chamber is pressure monitored to ensure a perfect seal.

2.3. Temperature testing and performance of the variable temperature cell

The temperature sensors used in this study were factory calibrated using a two-point calibration method. In addition to this, we have calibrated them in our lab using an additional Lakeshore 330 temperature monitoring unit provided with a calibrated and certified platinum resistor. Polynomial calibration curves were determined for each temperature sensor and entered in the LabVIEW software.

The temperature performance of the cell was tested through a sequence of measurements at different temperatures. The temperature readings and the standard deviations for each sensor are presented in Table 1. The standard deviation was determined using 1000 data points. Also included is the maximum difference between each two temperature sensors. The performance of our cell is better at temperatures above 273 K where all sensors agree within about 0.3 K. For temperatures below 273 K the agreement is slightly less with a maximum temperature difference of 0.4 K. The temperature stability in time has also been tested using readings over 5000 data points. Thermal stability is achieved within less than 20 min of reaching the chosen temperature where the extreme temperatures require a cooling process that can last at least 30 min.

2.4. Instrument control and monitoring software

We have used LabVIEW to automate and collect data using our experimental setup, presented in Fig. 3. A front panel screen accompanying the block diagram constitutes the program's graphical user interface. The program currently operates using a New Focus Velocity laser system that incorporates a Littman-Metcalf design allowing a tunability of 30 GHz in the 1500–1570 nm spectral range. The non-linearity of the piezo element has been corrected through the inclusion of a Fabry Perot interferometer that has a 1.5 GHz (or 0.05 cm⁻¹) free spectral range. This method allows us to record reliable wavelength scales. The interface of the laser virtual instrument allows the user either to select the desired wavelength to scan or enables the user to select specific transitions to be scanned. Table 2 presents the experimental conditions for all self-broadened acetylene spectra used in this study.

Table 1
Temperature performance in K for the five platinum resistor sensors mounted within the gas cell over a varying range of temperatures. Standard deviations are given in parentheses.

Sensor 1 6", left side	Sensor 2 18", left side	Sensor 3 30", left side	Sensor 4 6", right side	Sensor 5 18", right side	Maximum difference
332.865(5)	333.021(6)	332.866(4)	332.831(5)	332.938(11)	0.19
323.069(4)	323.154(7)	323.134(5)	323.017(5)	323.068(11)	0.14
313.013(51)	313.084(22)	312.776(13)	312.950(44)	313.022(14)	0.31
302.995(10)	302.978(7)	302.980(6)	302.952(9)	302.949(9)	0.05
293.191(3)	293.145(6)	292.965(5)	293.195(5)	293.149(10)	0.23
283.079(3)	283.207(6)	283.348(5)	283.221(4)	283.107(9)	0.27
273.042(44)	273.049(31)	272.939(13)	273.076(36)	273.116(12)	0.18
263.422(16)	263.429(7)	263.593(5)	263.547(11)	263.363(8)	0.23
253.707(20)	253.525(6)	253.766(5)	253.652(8)	253.509(8)	0.26
248.903(25)	248.847(62)	249.005(18)	248.923(9)	248.651(9)	0.35
244.145(8)	243.783(13)	243.797(6)	243.861(7)	243.879(11)	0.36
234.152(8)	233.841(8)	233.920(2)	233.939(9)	233.762(8)	0.39
225.013(7)	225.014(15)	225.006(29)	224.696(8)	224.784(22)	0.32
214.675(89)	214.840(93)	214.824(98)	214.469(105)	214.654(85)	0.37

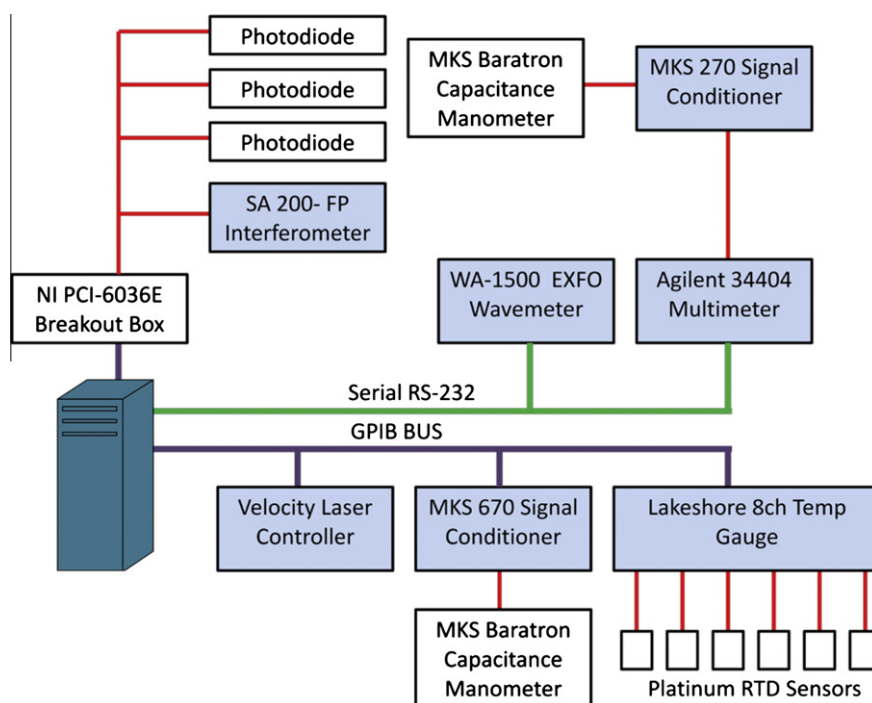


Fig. 3. Block diagram of the LabVIEW software used to monitor the instrumentation.

We have developed a series of programs designed to monitor and log the temperature and pressure data from our temperature controlled gas cell facility. Analog signals are carried along the red lines shown in Fig. 3 and are digitized by a National Instruments 6036E Multifunction 16 channel 16-bit DIO card. Serial connections are represented in green, and the IEEE 488 (GPIB) bus connection is represented by the violet line. A Windows XP-based PC running National Instruments LabVIEW 8.0 can communicate with each piece of test equipment colored blue. The three detectors used produce analog signals that are read via the 6036E card. The signal from the Baratron pressure gauge on channel 2 is digitized with an Agilent 34401A multimeter at 1 mV accuracy (or six digits of accuracy), and is interfaced to the LabVIEW computer over a RS-232 serial link. The second Baratron pressure gauge on channel 1 is connected to a 670 signal conditioner and is read using an IEEE 488 interface. The six temperature sensors are sampled via a Lakeshore model 218 temperature monitor. The unit has an electronic accuracy of ± 135 mK at 300 K.

A scan is performed with our instrument by setting the lasers center wavelength to the desired starting wavelength. Once the center wavelength has been set we measure pressure and temperature of the cell. Next, the piezo voltage is ramped from -3 V up to 2.7 V (which corresponds to a window of just over 30 GHz) in a user set interval usually around 0.001 V. At each step and for each detector we record the average and standard deviation of 100 points. At the end of the piezo scan we measure pressure and temperature again then repeat the process for a new center wavelength.

The analysis of the recorded spectral files is completed by first creating a wavelength scale using the information obtained from the wavemeter and the positions of the Fabry Perot peaks. Once the wavelength scale has been determined for a piezo scan, then a transmission file can be created. To create the transmission file we compare the baseline in the spectrum recorded on channel 1 or 2 with that of the third reference channel. The comparison is done by calculating a residual between the two spectra.

Table 2
Experimental conditions for our self-broadened acetylene spectra.

Lines scanned	Average pressure (Torr)	Average temperature (K)
R19-R0	107.08(19)	253.0(2)
R19-R0	108.45(3)	253.1(2)
R19-R0	265.09(3)	253.1(2)
R19-R0	377.88(1)	253.0(2)
R19-R0	377.88(1)	253.0(2)
R19-R0	538.79(9)	253.1(2)
R19-R0	649.07(20)	253.3(3)
R19-R0	648.89(2)	253.2(2)
R19-R0	780.12(7)	253.0(2)
R19-R0	98.42(2)	233.1(3)
R19-R0	98.48(2)	233.1(3)
R19-R0	244.33(7)	233.3(2)
R19-R4	371.70(9)	233.0(3)
R19-R0	371.84(1)	233.0(3)
R3-R0	371.82(0)	233.0(3)
R19-R0	486.50(23)	233.5(3)
R19-R0	486.54(3)	233.6(4)
R19-R0	595.34(10)	233.7(4)
R19-R0	595.48(6)	233.7(4)
R19-R0	713.10(17)	233.3(2)
R19-R0	90.52(17)	213.1(4)
R19-R0	90.09(6)	213.1(4)
R19-R0	221.57(5)	213.5(4)
R19-R0	337.39(8)	213.9(8)
R19-R0	337.11(3)	213.8(8)
R19-R0	337.25(1)	213.8(8)
R19-R0	337.19(1)	213.8(8)
R19-R0	442.08(6)	213.5(4)
R19-R0	441.86(6)	213.5(4)
R19-R0	541.05(19)	214.7(8)
R19-R0	540.83(1)	214.6(8)
R19-R0	645.95(22)	213.4(3)
R19-R0	645.68(2)	213.3(3)
R19-R0	645.48(13)	213.3(3)
R19-R0	574.67(1)	272.9(2)
R19-R0	115.02(1)	272.8(1)
R19-R0	115.58(21)	272.8(1)
R19-R0	247.19(23)	272.9(2)
R19-R0	434.10(1)	272.4(2)
R19-R0	434.12(1)	272.4(2)
R19-R0	483.70(4)	272.9(2)
R19-R0	483.70(1)	272.9(2)
R19-R0	574.70(3)	272.9(2)
R19-R0	700.01(3)	272.9(2)
R19-R0	700.09(2)	272.9(2)
R19-R0	93.50(8)	293.0(2)
R19-R0	93.86(8)	293.0(2)
R19-R0	264.71(5)	293.0(2)
R19-R0	436.52(1)	293.0(2)
R19-R0	436.56(1)	293.0(2)
R19-R0	519.22(1)	293.0(2)
R19-R0	519.23(1)	293.0(2)
R19-R0	616.59(1)	293.0(2)
R19-R0	616.57(3)	293.0(2)
R19-R0	751.27(1)	293.0(2)
R19-R0	751.34(3)	293.0(2)
R19-R0	100.41(6)	312.8(2)
R19-R0	100.31(1)	312.8(2)
R19-R0	230.09(4)	312.8(2)
R19-R0	385.03(1)	312.8(2)
R19-R0	385.08(1)	312.8(2)
R19-R0	496.36(1)	312.8(2)
R19-R0	496.38(1)	312.8(2)
R19-R0	496.39(1)	312.8(2)
R19-R0	496.36(0)	312.8(2)
R19-R0	593.06(1)	312.8(2)
R19-R0	593.03(1)	312.8(2)
R19-R0	679.55(2)	312.8(2)
R19-R0	679.47(1)	312.8(2)
R19-R0	106.68(4)	332.7(2)
R19-R0	106.78(1)	332.7(2)
R19-R0	244.43(15)	332.6(2)
R19-R0	409.04(1)	332.7(2)
R19-R0	409.05(1)	332.7(2)

Table 2 (continued)

Lines scanned	Average pressure (Torr)	Average temperature (K)
R19-R0	527.04(4)	332.6(2)
R19-R0	527.15(3)	332.7(2)
R19-R0	630.17(1)	332.6(2)
R19-R0	630.15(1)	332.6(2)
R19-R0	721.96(4)	332.6(2)
R19-R0	721.91(5)	332.6(2)
R19-R0	107.08(19)	253.0(2)

$$\text{residual} = \text{Channel1 baseline} - \text{Channel3 background} \quad (1)$$

Channel1 baseline refers to the spectra measured on channel 1 with the lines cut from the file. We then take the residual and fit a Chebyshev polynomial to it. Once we have found the best order of Chebyshev polynomial we then correct the channel 3 background signal using the following equation:

$$\text{Cheb Poly} + \text{Channel3 background} = \text{Corrected baseline} \quad (2)$$

With this corrected baseline we are then able to divide the channel 1 or 2 spectra by the background to get a transmission spectral file. Individual or groups of spectra were fitted with the Voigt or speed-dependent Voigt profiles using software developed by Hurtmans [36].

To confirm the good quality of the data obtained with our instrument we carefully examined our ability to locate the line positions of the transitions and then compared our fitted values for selected transitions to those found in Ref. [1] and HITRAN 2008 [37]. We examined seven low pressure spectra recorded nearby the P(21) line of the $\nu_1 + \nu_3$ band. This band was ideal because of its intense and accurate line positions are available [37]. Each spectrum was recorded at approximately 40 mTorr with measurements on channel 1 of Fig. 1 being 43 mTorr and channel 2 being 40 mTorr. Fits performed on these spectra revealed line positions with an average difference from HITRAN 2008 of about 0.002288 cm^{-1} , and compared to values reported by Madej et al. [1] with an average difference of 0.002275 cm^{-1} . These values are comparable to the combined error of about 0.001664 cm^{-1} associated with the combination of wavemeter and FP cavity.

We also examined the difference in the line positions as determined from both channels 1 and 2 to see if there were any phase differences from the data sampling or other systematic errors. Spectral line fits for line positions for spectra recorded using both channels 1 and 2 were found to have an average difference in line positions of $0.0000165 \text{ cm}^{-1}$. This value is equivalent to the error associated with the fitting routine [36], thus suggesting that we are able to perform simultaneous and accurate measurements using both channels of our system. The calibration procedure used in this study allowed us to determine accurate wavenumber scales for each spectrum and consequently retrieve accurate pressure shift values.

3. Data analysis and interpretation of results

The $\nu_1 + \nu_2 + \nu_4 + \nu_5$ upper state in $^{12}\text{C}_2\text{H}_2$ has three sub-states, of Σ_u^+ , Σ_u^+ , Π symmetry. The band investigated here is parallel with P and R branches only. The upper sub-state belongs to the $\{\text{Nr}, \text{Ns}, e, u\} = \{10, 2, e, u\}$ polyad with $\text{Nr} = 5\nu_1 + 5\nu_3 + 3\nu_2 + \nu_4 + \nu_5$ and $\text{Ns} = \nu_1 + \nu_2 + \nu_3$. The nuclear spin statistics are either 1 or 3 for even or odd lower J values, respectively (the opposite for the upper J values). Further details on the ground state structure in acetylene can be found in Ref. [38].

The line parameters of acetylene were retrieved using a weighted multispectrum analysis software [36]. The spectra were

divided in smaller sections covering each of the R(0) to R(19) transitions. Batches of spectra recorded at the same set temperature were fitted together. The program minimized the differences between the experimental spectra and the calculated spectra by adjusting various line parameters through non-linear least squares. For the transitions presented in this work, line mixing was needed to fit the spectra within the noise levels. Initial values for the line intensities, self-broadened widths were taken from Ref. [37]. Two lineshape models were used in our work: Voigt and speed-dependent Voigt. The spectral line parameters of interest to us in the present study are line intensities, linewidths, pressure shifts and weak line mixing coefficients.

3.1. Line intensities

For each transition from R(0) to R(19) we have retrieved the line intensities at all set temperatures by simultaneously analyzing the spectra with the multispectrum fit program [36]. The line intensities retrieved by fitting to Voigt and speed-dependent Voigt are

presented in Tables 3A and 3B, respectively. The errors quoted in paranthesis are double the fit errors. Based on consistency tests applied to different lines, we believe that our intensities are accurate to better than 2%.

For an easy comparison of our results with results available in the literature reported at 296 K, we converted our room temperature intensities to intensities at 296 K using the formula:

$$S_{j'}(T_0) = S_{j'}(T_1)T_1/T_0(Z(T_0))/(Z(T_1))\exp\{-(hcE_{j'})/k(1/T_0 - 1/T_1)\} \quad (3)$$

where T_1 is the individual temperature of our spectra, T_0 is 296 K and $E_{j'}$ are the lower state energies reported in the HITRAN 2008 database [37] and the partition functions were assumed to be nearly the same for temperature variations up to 3 K. The converted intensities given in $\text{cm} \times \text{molecule}^{-1}$ are available in Tables 3A and 3B, corresponding to fits with the Voigt or speed-dependent Voigt profiles. In Fig. 4 we have plotted the ratios between our converted intensities at 296 K and the HITRAN 2008 [37] values. With two exceptions, all ratios are below 1. In fact, the average ratio for inten-

Table 3A
Line intensities in the $\nu_1 + \nu_2 + \nu_4 + \nu_5$ band of acetylene determined using the Voigt profile.

Line	m	213 K	233 K	253 K	273 K	293 K	$R^2 (D^2 \times 10^6)$	318 K	350 K	296 K	$R^2 (D^2 \times 10^6)$
<i>Intensity $\times 10^{24}$ (cm molecule$^{-1}$) retrieved with the Voigt profile</i>											
R(0)	1	12.91(1)	12.01(2)	11.10(1)	10.23(1)	9.50(2)	1.38(3)	8.90(2)	8.87(5)	9.39(2)	1.37(3)
R(1)	2	78.80(1)	73.48(1)	67.78(1)	62.12(1)	56.92(2)	1.39(3)	51.72(2)	48.43(4)	56.13(2)	1.39(3)
R(2)	3	38.03(1)	35.68(1)	33.07(2)	30.41(2)	27.86(2)	1.39(3)	25.13(1)	22.90(2)	27.47(1)	1.39(3)
R(3)	4	145.44(1)	136.49(2)	126.70(4)	116.80(3)	107.50(1)	1.39(3)	97.84(2)	90.74(3)	106.04(2)	1.39(3)
R(4)	5	57.18(1)	54.24(1)	50.85(1)	47.26(1)	43.69(1)	1.42(3)	39.62(1)	35.72(1)	43.10(1)	1.42(3)
R(5)	6	191.27(2)	180.60(3)	168.75(2)	156.62(3)	145.09(2)	1.39(3)	132.87(2)	123.39(2)	143.19(2)	1.38(3)
R(6)	7	68.65(1)	65.00(1)	60.93(1)	56.76(1)	52.81(1)	1.39(3)	48.64(1)	45.50(1)	52.13(1)	1.43(3)
R(7)	8	208.93(2)	199.36(2)	188.33(3)	176.69(1)	165.27(1)	1.38(3)	152.61(2)	141.47(1)	163.21(2)	1.37(3)
R(8)	9	70.19(1)	67.42(1)	64.13(1)	60.58(1)	57.02(5)	1.39(3)	52.96(1)	49.13(1)	56.34(1)	1.38(3)
R(9)	10	201.90(3)	195.27(3)	187.11(3)	178.11(3)	168.93(1)	1.37(3)	158.26(2)	147.86(2)	166.99(2)	1.37(3)
R(10)	11	64.61(1)	62.89(1)	60.65(6)	58.09(2)	55.41(3)	1.38(3)	52.19(7)	48.84(6)	54.80(3)	1.36(3)
R(11)	12	179.14(2)	175.57(2)	170.58(7)	164.66(2)	158.31(6)	1.36(3)	150.50(1)	142.18(15)	156.65(1)	1.35(3)
R(12)	13	54.24(1)	53.61(1)	52.56(1)	51.21(2)	49.71(1)	1.36(3)	47.80(2)	45.70(7)	49.22(2)	1.35(3)
R(13)	14	143.64(1)	143.81(1)	142.66(3)	140.41(1)	137.28(4)	1.35(3)	132.50(3)	125.61(5)	135.99(3)	1.34(3)
R(14)	15	42.03(1)	42.47(1)	42.50(1)	42.18(1)	41.55(3)	1.35(3)	40.42(2)	38.52(8)	41.19(2)	1.34(3)
R(15)	16	106.28(2)	109.46(1)	111.41(3)	112.13(3)	111.61(4)	1.34(3)	109.17(1)	103.14(3)	110.68(3)	1.32(3)
R(16)	17	30.42(1)	31.43(1)	32.15(1)	32.56(2)	32.68(1)	1.33(3)	32.41(3)	31.40(3)	32.43(2)	1.32(3)
R(17)	18	74.85(2)	78.56(1)	81.48(2)	83.54(2)	84.71(2)	1.33(3)	84.81(2)	82.60(3)	84.12(2)	1.31(3)
R(18)	19	19.92(1)	21.39(1)	22.62(1)	23.58(2)	24.21(2)	1.32(3)	24.49(1)	23.90(2)	24.06(1)	1.30(3)
R(19)	20	48.93(1)	52.72(1)	56.00(1)	58.67(1)	60.67(2)	1.31(3)	62.05(3)	61.78(2)	60.33(1)	1.28(3)

Table 3B
Line intensities in the $\nu_1 + \nu_2 + \nu_4 + \nu_5$ band of acetylene determined using the speed dependent Voigt profile.

Line	m	213 K	233 K	253 K	273 K	293 K	$R^2 (D^2 \times 10^6)$	318 K	350 K	296 K	$R^2 (D^2 \times 10^6)$
<i>Intensity $\times 10^{24}$ (cm molecule$^{-1}$) retrieved with the speed-dependent Voigt profile</i>											
R(0)	1	12.94(1)	12.03(2)	11.09(1)	10.21(1)	9.48(3)	1.38(3)	8.90(2)	8.92(6)	9.34(2)	1.38(3)
R(1)	2	79.03(1)	73.69(2)	67.96(1)	62.28(1)	57.06(1)	1.40(3)	51.85(2)	48.57(4)	56.18(1)	1.39(3)
R(2)	3	38.14(1)	35.77(1)	33.15(2)	30.47(1)	27.92(2)	1.40(3)	25.20(1)	22.99(2)	27.49(1)	1.39(3)
R(3)	4	145.62(3)	136.69(2)	126.92(3)	117.03(3)	107.75(1)	1.39(3)	98.11(2)	91.05(3)	106.09(1)	1.39(3)
R(4)	5	57.45(1)	54.29(1)	50.78(2)	47.19(1)	43.78(1)	1.42(3)	40.17(1)	37.39(1)	43.10(2)	1.42(3)
R(5)	6	191.61(2)	180.89(3)	169.00(2)	156.82(3)	145.25(2)	1.39(3)	133.01(2)	123.52(2)	142.39(2)	1.39(3)
R(6)	7	69.13(1)	65.17(1)	60.57(1)	56.37(1)	52.52(1)	1.38(3)	48.30(1)	44.16(1)	53.59(1)	1.39(3)
R(7)	8	209.36(3)	199.73(2)	188.65(3)	176.96(1)	165.52(1)	1.38(3)	152.84(2)	141.75(1)	162.96(2)	1.38(3)
R(8)	9	70.37(1)	67.59(1)	64.28(1)	60.72(1)	57.14(5)	1.39(3)	53.05(1)	49.19(1)	56.26(1)	1.39(3)
R(9)	10	202.21(3)	195.95(3)	188.07(4)	179.22(4)	170.03(4)	1.38(3)	159.07(2)	147.77(2)	167.41(1)	1.37(3)
R(10)	11	64.70(1)	63.03(2)	60.79(2)	58.17(2)	55.34(2)	1.37(3)	51.80(3)	47.77(2)	54.49(4)	1.37(3)
R(11)	12	179.47(2)	176.11(2)	171.21(3)	165.23(6)	158.64(3)	1.37(3)	150.24(1)	140.55(1)	156.28(3)	1.36(3)
R(12)	13	54.43(1)	53.81(1)	52.75(1)	51.39(1)	49.85(1)	1.36(3)	47.88(2)	45.67(2)	49.19(4)	1.35(3)
R(13)	14	144.08(3)	144.13(3)	142.88(5)	140.57(3)	137.43(4)	1.35(3)	132.71(3)	126.10(4)	135.73(1)	1.34(3)
R(14)	15	42.09(1)	42.59(1)	42.67(1)	42.35(2)	41.69(3)	1.35(3)	40.42(2)	38.22(2)	41.20(1)	1.34(3)
R(15)	16	106.87(3)	109.71(3)	111.37(3)	111.86(3)	111.21(4)	1.34(3)	108.78(3)	103.12(3)	110.06(1)	1.33(3)
R(16)	17	30.59(1)	31.56(1)	32.23(1)	32.61(2)	32.70(1)	1.34(3)	32.44(2)	31.49(3)	32.41(2)	1.32(3)
R(17)	18	75.19(2)	78.65(2)	81.35(2)	83.28(2)	84.39(2)	1.32(3)	84.60(2)	82.86(3)	83.76(2)	1.31(3)
R(18)	19	20.18(1)	21.46(1)	22.54(1)	23.40(1)	24.01(2)	1.31(3)	24.41(1)	24.25(2)	23.88(1)	1.31(3)
R(19)	20	49.30(1)	52.64(1)	55.56(1)	58.01(2)	59.93(2)	1.29(3)	61.53(1)	62.12(2)	59.66(3)	1.29(3)

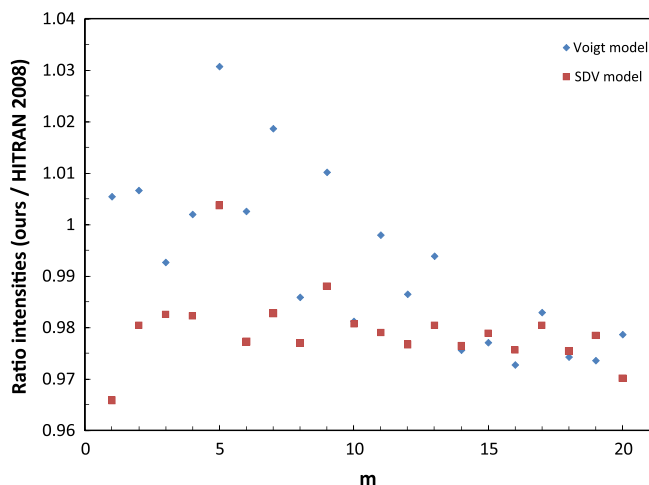


Fig. 4. Ratios between our intensities at 296 K and the values from HITRAN 2008 [31].

sities retrieved using the speed dependent Voigt profile is 0.986575, and for intensities retrieved using the Voigt profile is 0.986512. Overall, our intensity measurements are in good agreement with HITRAN 2008.

We have calculated the transition dipole moment squared $|R|^2$ (in Debye²) using the following expression:

$$S_{J''}(T) = \frac{1}{4\pi\epsilon_0} \frac{8\pi^3}{3hc} \frac{\nu}{Z(T)} \times \exp\left\{-\frac{cE_{J''}}{kT}\right\} \left[1 - \exp\left\{-\frac{hc\nu}{kT}\right\}\right] |R|^2 L(J'', l) \frac{g_s}{g_l} \quad (4)$$

where h is the Planck's constant, c is the speed of light, g_s is the statistical weight due to nuclear spin of the lower level, ν is the transition wavenumber in cm^{-1} ; g_l is a weight introduced in case of bands with l -type doubling; $Z(T)$ is the total partition function at temperature T ; $L(J'', l)$ is the Hönl–London factor, J'' being the rotational quantum number of the lower level of the transition, and l its secondary vibrational quantum number ($l = |l_4 + l_5|$ for C_2H_2); E'' in cm^{-1} , is the energy of the lower level; k is Boltzmann's constant.

Our band is a parallel band with $l = 0$. For R branch transitions the factor is:

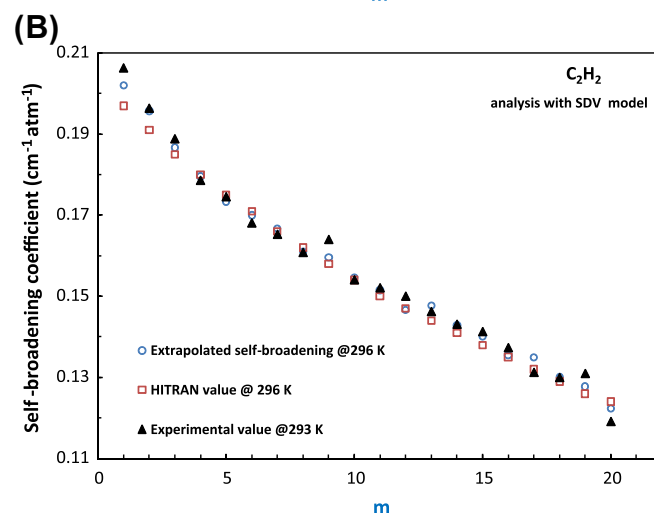
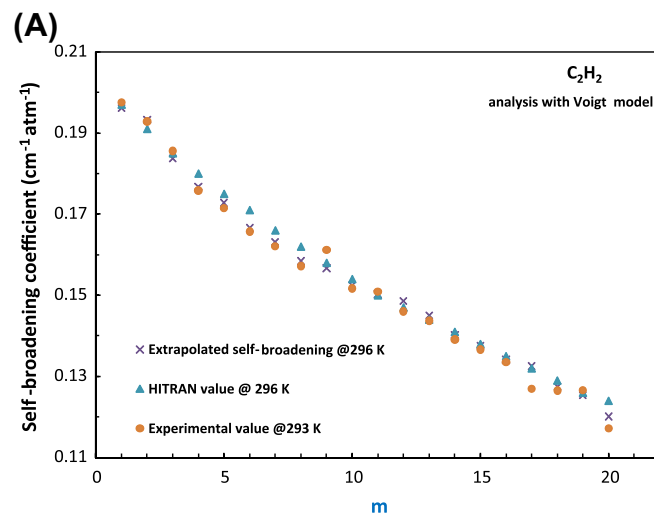


Fig. 5. Room temperature self-broadening coefficients retrieved using the Voigt profile (panel A) and speed dependent Voigt profile (B).

$$L(J'', l) = (J'' + 1 + l)(J'' + 1 - l)/(J'' + 1) \quad (5)$$

The measured values for $|R|^2$ for the 20 lines are next fitted through a least squares procedure to the following equation:

Table 4A

Self-broadening coefficients in the $\nu_1 + \nu_2 + \nu_4 + \nu_5$ band of acetylene determined using the Voigt profile.

Line	m	213 K	233 K	253 K	273 K	293 K	318 K	350 K	296 K
<i>Self-broadening coefficients ($\text{cm}^{-1} \text{atm}^{-1}$) retrieved with the Voigt profile</i>									
R(0)	1	0.24041(3)	0.22757(9)	0.21656(6)	0.20065(12)	0.19763(7)	0.18406(8)	0.17873(6)	0.1962(2)
R(1)	2	0.23885(3)	0.22476(8)	0.21315(6)	0.20273(11)	0.19292(7)	0.17952(8)	0.17652(6)	0.1933(2)
R(2)	3	0.22201(2)	0.21167(8)	0.20676(6)	0.19084(11)	0.1856(6)	0.17337(7)	0.16471(6)	0.1837(2)
R(3)	4	0.2137(4)	0.20202(7)	0.19362(5)	0.18546(10)	0.17585(6)	0.16829(7)	0.16108(6)	0.1768(2)
R(4)	5	0.21061(2)	0.19837(6)	0.18606(5)	0.1794(9)	0.17155(6)	0.16518(6)	0.15956(6)	0.1728(2)
R(5)	6	0.2028(5)	0.19377(3)	0.18055(4)	0.17263(9)	0.16576(4)	0.15902(4)	0.1513(3)	0.1666(2)
R(6)	7	0.20013(8)	0.18807(10)	0.17704(4)	0.17018(10)	0.16209(6)	0.15604(9)	0.14847(7)	0.1631(2)
R(7)	8	0.19588(4)	0.18278(2)	0.17292(4)	0.16509(4)	0.15722(2)	0.15016(2)	0.14305(3)	0.1584(2)
R(8)	9	0.19301(3)	0.18072(6)	0.16964(6)	0.16203(5)	0.16122(10)	0.14877(5)	0.1415(11)	0.1566(2)
R(9)	10	0.18804(5)	0.17799(1)	0.16725(4)	0.15736(3)	0.15171(5)	0.14499(4)	0.13925(8)	0.1524(2)
R(10)	11	0.18458(2)	0.17251(2)	0.16779(2)	0.15572(2)	0.15096(3)	0.13909(3)	0.13656(2)	0.1503(2)
R(11)	12	0.18271(6)	0.17077(2)	0.16227(2)	0.1542(3)	0.14602(3)	0.14172(2)	0.13737(3)	0.1486(1)
R(12)	13	0.17493(3)	0.16389(2)	0.15691(2)	0.14801(3)	0.14371(3)	0.14254(3)	0.13474(4)	0.1451(1)
R(13)	14	0.16944(3)	0.15934(3)	0.15212(5)	0.14602(2)	0.13909(3)	0.13643(2)	0.12818(3)	0.1402(1)
R(14)	15	0.16775(6)	0.15409(5)	0.14965(3)	0.14373(4)	0.1366(3)	0.13361(5)	0.1258(17)	0.1375(1)
R(15)	16	0.15902(3)	0.15083(3)	0.14527(2)	0.14066(2)	0.13352(3)	0.13022(3)	0.11992(5)	0.1341(1)
R(16)	17	0.15715(3)	0.14965(2)	0.14152(3)	0.1387(1)	0.12698(7)	0.12923(7)	0.12131(6)	0.1325(1)
R(17)	18	0.15179(2)	0.14553(2)	0.13534(3)	0.13222(1)	0.12649(2)	0.12315(2)	0.11805(6)	0.1275(1)
R(18)	19	0.14759(6)	0.13962(7)	0.13348(5)	0.12943(1)	0.12657(4)	0.12037(4)	0.11721(3)	0.1253(1)
R(19)	20	0.14491(3)	0.13633(4)	0.13005(3)	0.12341(3)	0.11723(3)	0.11286(3)	0.11287(5)	0.1201(1)

Table 4B
Self-broadening coefficients in the $\nu_1 + \nu_2 + \nu_4 + \nu_5$ band of acetylene determined using the speed dependent Voigt profile.

Line	m	213 K	233 K	253 K	273 K	293 K	318 K	350 K	296 K
<i>Self-broadening coefficients ($\text{cm}^{-1} \text{atm}^{-1}$) retrieved with the speed-dependent Voigt profile</i>									
R(0)	1	0.24908(31)	0.23579(43)	0.22312(18)	0.21216(22)	0.20625(44)	0.19029(6)	0.18489(9)	0.2020(2)
R(1)	2	0.24649(6)	0.22866(7)	0.22045(5)	0.20901(6)	0.19632(6)	0.18333(7)	0.17991(13)	0.1957(2)
R(2)	3	0.22913(8)	0.21482(8)	0.21295(16)	0.19622(10)	0.18878(11)	0.17686(8)	0.16799(16)	0.1866(2)
R(3)	4	0.21851(8)	0.20506(6)	0.19814(9)	0.19009(6)	0.17854(3)	0.17124(4)	0.16392(5)	0.1796(2)
R(4)	5	0.21709(8)	0.20156(7)	0.19137(8)	0.18418(7)	0.17450(5)	0.16811(6)	0.15956(6)	0.1733(2)
R(5)	6	0.20713(5)	0.19629(8)	0.18460(4)	0.17635(5)	0.16804(3)	0.16122(4)	0.15329(3)	0.1699(2)
R(6)	7	0.2060(6)	0.19119(5)	0.18246(5)	0.17495(4)	0.16524(4)	0.15896(5)	0.15110(5)	0.1667(2)
R(7)	8	0.19998(5)	0.18504(4)	0.17683(2)	0.16695(2)	0.16077(2)	0.15221(2)	0.14502(2)	0.1610(2)
R(8)	9	0.19845(5)	0.18367(5)	0.17461(5)	0.16685(5)	0.16398(17)	0.15122(4)	0.14374(5)	0.1596(2)
R(9)	10	0.19192(6)	0.18024(6)	0.17099(6)	0.16100(0)	0.15404(6)	0.14723(3)	0.14162(3)	0.1546(2)
R(10)	11	0.18570(0)	0.17602(6)	0.17016(5)	0.15758(6)	0.15207(6)	0.14420(6)	0.13440(0)	0.1515(2)
R(11)	12	0.18675(4)	0.17288(4)	0.16670(4)	0.13500(6)	0.15000(6)	0.14200(3)	0.13610(1)	0.1466(1)
R(12)	13	0.17998(7)	0.16657(6)	0.16212(6)	0.15354(5)	0.14621(4)	0.14260(6)	0.13807(4)	0.1477(1)
R(13)	14	0.17365(6)	0.16313(5)	0.15441(8)	0.14936(5)	0.14309(5)	0.13620(4)	0.13146(5)	0.1428(1)
R(14)	15	0.17176(6)	0.15665(6)	0.15486(5)	0.14827(8)	0.14127(10)	0.13702(9)	0.12494(9)	0.1401(1)
R(15)	16	0.16324(7)	0.15301(7)	0.14955(5)	0.14449(6)	0.13731(7)	0.13089(5)	0.12175(6)	0.1354(1)
R(16)	17	0.16315(5)	0.15216(5)	0.14532(7)	0.14348(8)	0.13123(8)	0.13077(12)	0.12364(15)	0.1349(1)
R(17)	18	0.15614(4)	0.14672(6)	0.13933(5)	0.13596(4)	0.12996(4)	0.12553(4)	0.12057(6)	0.1300(1)
R(18)	19	0.14759(6)	0.14213(6)	0.13806(8)	0.13245(10)	0.13094(12)	0.12272(8)	0.12051(12)	0.1277(1)
R(19)	20	0.14920(4)	0.13853(4)	0.13384(4)	0.12515(5)	0.11912(5)	0.11522(4)	0.11509(5)	0.1223(1)

Table 5A
Pressure induced line self-shift coefficients in the $\nu_1 + \nu_2 + \nu_4 + \nu_5$ band of acetylene determined using the Voigt profile.

Line	m	213 K	233 K	253 K	273 K	293 K	318 K	350 K	296 K
<i>Self-shifting coefficients ($\text{cm}^{-1} \text{atm}^{-1}$) retrieved with the Voigt profile</i>									
R(0)	1								
R(1)	2	-0.00147(3)	0.00411(7)	0.00056(3)	-0.00400(10)	-0.00122(5)	0.00077(5)	-0.00071(5)	-0.00108(2)
R(2)	3	0.00166(3)	-0.00042(6)	0.00202(3)	-0.00078(9)	-0.00145(5)	-0.00319(5)	-0.00483(5)	-0.00221(2)
R(3)	4	-0.00261(3)	-0.00112(6)	-0.00027(4)	-0.00202(8)	-0.00157(5)	-0.00283(5)	-0.00332(4)	-0.00214(2)
R(4)	5	-0.00441(3)	-0.00273(5)	-0.00160(4)	-0.00493(7)	-0.00452(5)	-0.00536(4)	-0.00497(4)	-0.00447(4)
R(5)	6	-0.00472(4)	-0.00312(2)	-0.00469(2)	-0.00429(5)	-0.00450(4)	-0.00416(4)	-0.00362(2)	-0.00423(4)
R(6)	7	-0.00563(5)	-0.00607(8)	-0.00422(3)	-0.00796(8)	-0.00501(6)	-0.00660(6)	-0.00413(7)	-0.00570(5)
R(7)	8	-0.00656(4)	-0.00574(2)	-0.00566(3)	-0.00607(3)	-0.00521(2)	-0.00451(2)	-0.00482(2)	-0.00481(4)
R(8)	9	-0.00711(3)	-0.00608(5)	-0.00677(10)	-0.00670(4)	-0.00883(6)	-0.00414(5)	-0.00771(6)	-0.00510(6)
R(9)	10	-0.00550(2)	-0.00488(1)	-0.00725(4)	-0.00805(2)	-0.00518(3)	-0.00601(4)	-0.00687(3)	-0.00617(6)
R(10)	11	-0.00892(2)	-0.00750(2)	-0.00760(2)	-0.00705(2)	-0.00608(3)	-0.00518(2)	-0.00765(2)	-0.00580(6)
R(11)	12	-0.00992(1)	-0.00820(2)	-0.00691(2)	-0.00708(3)	-0.00554(2)	-0.00674(2)	-0.00818(3)	-0.00567(6)
R(12)	13	-0.00914(2)	-0.00853(2)	-0.00637(1)	-0.00730(3)	-0.00759(3)	-0.00361(2)	-0.00505(3)	-0.00578(6)
R(13)	14	-0.01235(3)	-0.01100(2)	-0.01037(4)	-0.00803(2)	-0.00697(2)	-0.00713(2)	-0.00424(3)	-0.00730(8)
R(14)	15	-0.01159(4)	-0.01073(5)	-0.00957(3)	-0.00892(4)	-0.00732(3)	-0.00774(3)	-0.00650(11)	-0.00809(8)
R(15)	16	-0.01270(3)	-0.01130(2)	-0.01059(2)	-0.00918(2)	-0.00925(3)	-0.00833(2)	-0.00506(4)	-0.00890(8)
R(16)	17	-0.01444(7)	-0.01276(3)	-0.01330(1)	-0.01059(1)	-0.01078(3)	-0.01240(3)	-0.00841(2)	-0.01011(10)
R(17)	18	-0.01306(3)	-0.01160(3)	-0.01165(3)	-0.01048(4)	-0.01016(3)	-0.00895(2)	-0.00828(3)	-0.00974(10)
R(18)	19	-0.01419(4)	-0.01377(4)	-0.01179(2)	-0.01174(2)	-0.01155(2)	-0.00972(2)	-0.00881(1)	-0.01062(10)
R(19)	20	-0.01468(2)	-0.01434(36)	-0.01422(2)	-0.01285(3)	-0.01193(2)	-0.01080(2)	-0.01001(-5)	-0.01169(12)

$$|R|^2 = |R_0|^2 F(m) = |R_0|^2 (1 + A_1 m + A_2 m^2) \quad (6)$$

where $|R_0|^2$ is the vibrational transition dipole moment squared, and $F(m)$ is the empirical Herman–Wallis factor. The Herman–Wallis factor can be expressed using the coefficients A_1 and A_2 and m (m is $J'' + 1$ for R branch transitions). The values for $|R_0|^2$, A_1 , A_2 for intensities at 293 K are: $1.39(1) \times 10^{-06} D^2$, $5.9(6) \times 10^{-04}$, $-9.6(3) \times 10^{-05}$ (Voigt model) and $1.39(1) \times 10^{-06} D^2$, $1.2(7) \times 10^{-03}$, $-1.3(3) \times 10^{-04}$ (SDV model). The values for $|R_0|^2$, A_1 , A_2 for intensities extrapolated to 296 K are: $1.390(11) \times 10^{-06} D^2$, $9.5(7) \times 10^{-04}$, $-1.4(4) \times 10^{-04}$ (Voigt model) and $1.394(1) \times 10^{-06} D^2$, $2.4(6) \times 10^{-04}$, $-9.6(2) \times 10^{-05}$ (SDV model).

3.2. Line broadening and pressure induced line shifts

The expressions used to retrieve the self-broadened half width and pressure induced shift coefficients and their temperature dependences are as follows:

$$\gamma(p, T) = p \gamma_0(p_0, T_0) \left[\frac{T_0}{T} \right]^n \quad (7)$$

$$\nu = \nu_0 + p \delta^0 \quad (8)$$

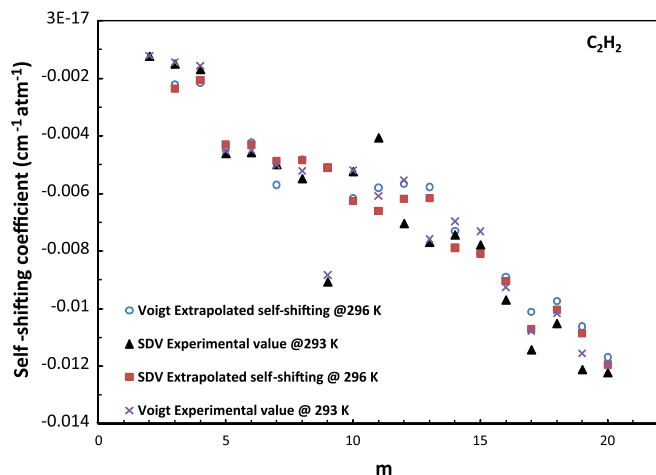
$$\delta^0(T) = \delta^0(T_0) + \delta'_0(T - T_0) \quad (9)$$

$$\delta^0(T) = \delta^0(p_0, T_0) \left[\frac{T_0}{T} \right]^n \quad (10)$$

where $p_0 = 1$ atm and $T_0 = 296$ K are the reference pressure and temperature. γ_0 is the retrieved self-broadened half-width coefficient at the reference pressure p_0 and temperature T_0 . $\gamma(p, T)$ is the measured self-broadened half width of the spectral line and p is the total pressure of the acetylene sample. n is the temperature dependence exponent of the self-broadened half-width coefficient. δ^0 is the pressure-induced line shift coefficient, ν is the line position, ν_0 is the position at zero pressure, and δ' is the temperature dependent coefficient of the self-induced pressure shift coefficients. Note that in this study we have explored a second law for temperature dependence of pressure shifts, namely Eq. (10).

Table 5BPressure induced line self-shift coefficients in the $\nu_1 + \nu_2 + \nu_4 + \nu_5$ band of acetylene determined using the speed dependent Voigt profile.

Line	m	213 K	233 K	253 K	273 K	293 K	318 K	350 K	296 K
<i>Self-broadening coefficients ($\text{cm}^{-1} \text{atm}^{-1}$) retrieved with the speed-dependent Voigt profile</i>									
R(0)	1	-0.00396(15)	0.0026(23)	-0.02544(12)	-0.00456(13)	-0.02717(34)	-0.00014(39)	-0.00237(47)	-0.0022(2)
R(1)	2	-0.00142(3)	0.00423(4)	0.00069(2)	-0.00415(3)	-0.00123(4)	0.0008(3)	-0.00066(7)	-0.00295(4)
R(2)	3	-0.00166(4)	-0.00047(6)	-0.002(10)	-0.00084(6)	-0.0015(7)	-0.00322(4)	-0.00487(8)	-0.00236(2)
R(3)	4	-0.00371(5)	-0.00121(4)	-0.00044(6)	-0.00228(4)	-0.00169(2)	-0.00303(2)	-0.00357(3)	-0.00205(2)
R(4)	5	-0.00464(5)	-0.00278(5)	-0.00169(5)	-0.00521(5)	-0.00461(3)	-0.00546(4)	-0.00497(4)	-0.0043(4)
R(5)	6	-0.00483(3)	-0.00316(3)	-0.00483(3)	-0.00446(4)	-0.00458(2)	-0.00423(3)	-0.00367(2)	-0.00431(4)
R(6)	7	-0.00582(3)	-0.00615(3)	-0.0043(3)	-0.00811(3)	-0.00499(3)	-0.00654(3)	-0.00408(3)	-0.00487(2)
R(7)	8	-0.00675(3)	-0.00584(2)	-0.00586(3)	-0.00621(2)	-0.00548(1)	-0.00457(2)	-0.00494(1)	-0.00484(2)
R(8)	9	-0.00734(3)	-0.0062(3)	-0.00699(3)	-0.00698(3)	-0.00906(2)	-0.0042(3)	-0.00783(3)	-0.0051(4)
R(9)	10	-0.00558(2)	-0.00492(4)	-0.00741(4)	-0.00721(3)	-0.00524(4)	-0.00607(2)	-0.00696(2)	-0.00626(4)
R(10)	11	-0.0096(3)	-0.00906(4)	-0.00772(3)	-0.00902(3)	-0.00406(3)	-0.00596(4)	-0.00357(3)	-0.00661(4)
R(11)	12	-0.01015(2)	-0.00829(3)	-0.00859(2)	-0.0082(5)	-0.00704(3)	-0.00644(2)	-0.00568(3)	-0.00618(4)
R(12)	13	-0.00939(4)	-0.00866(4)	-0.00664(3)	-0.00738(3)	-0.00769(3)	-0.00559(3)	-0.0057(2)	-0.00615(4)
R(13)	14	-0.01125(4)	-0.01053(3)	-0.0096(5)	-0.00872(3)	-0.00743(4)	-0.00384(3)	-0.00468(4)	-0.00789(4)
R(14)	15	-0.01175(3)	-0.01098(4)	-0.01006(3)	-0.00893(5)	-0.00778(6)	-0.0074(6)	-0.00954(6)	-0.0081(4)
R(15)	16	-0.01308(4)	-0.01256(4)	-0.01092(3)	-0.00945(4)	-0.00969(4)	-0.00878(3)	-0.00594(4)	-0.00905(6)
R(16)	17	-0.01602(3)	-0.01302(3)	-0.01523(4)	-0.01123(5)	-0.01142(5)	-0.01177(7)	-0.00871(9)	-0.01071(6)
R(17)	18	-0.01332(2)	-0.01167(4)	-0.01201(3)	-0.01081(2)	-0.01051(3)	-0.00939(2)	-0.00847(4)	-0.01004(6)
R(18)	19	-0.01419(4)	-0.01417(4)	-0.01224(4)	-0.01209(6)	-0.01211(7)	-0.00996(4)	-0.00819(7)	-0.01085(6)
R(19)	20	-0.01519(2)	-0.01461(2)	-0.01471(2)	-0.0124(3)	-0.01222(3)	-0.01102(3)	-0.01017(3)	-0.01196(8)

**Fig. 6.** Room temperature pressure induced self-shift coefficients obtained using the Voigt and speed-dependent Voigt profiles.

We have retrieved broadening coefficients using a multispectrum fitting procedure and the Voigt and speed-dependent Voigt profiles. The values retrieved for each temperature and those extrapolated for 296 K are given in Tables 4A and Fig. 5A for fits using the Voigt profile and Table 4B and Fig. 5B for fits using the speed-dependent Voigt profile. The errors quoted in parentheses are twice the errors from the multispectrum fits. Based on consistency tests performed on several lines, we believe that our broadening parameters are accurate to 1.5%. It can be noticed that the speed-dependent Voigt results are slightly larger than the Voigt ones. Our measurements are in good agreement with previous data sets for self-broadened acetylene.

The multispectrum fits allowed us to simultaneously retrieve the pressure-induced line shifts with the two line profiles. The results are presented in Tables 5A for Voigt results and 5B and Fig. 6 for speed-dependent Voigt results. The errors quoted in parentheses are twice the errors from the multispectrum fits. Fig. 6 shows little differences in the size of the two sets of shifts. We were also able to extrapolate the values for shifts to 296 K. These values are also reported in Tables 5A and 5B and plotted on Fig. 6.

We report our results for the temperature dependences of shifting coefficients plotted in Fig. 7 and reported in Table 6. Fig. 7 presents graphically the results obtained for temperature dependencies of pressure shifts when the empirical law from Eq. (10) is used (panel A) and when the empirical law from Eq. (9) is used (panel B). In the case of the Eq. (9) the δ'_0 become negative at very

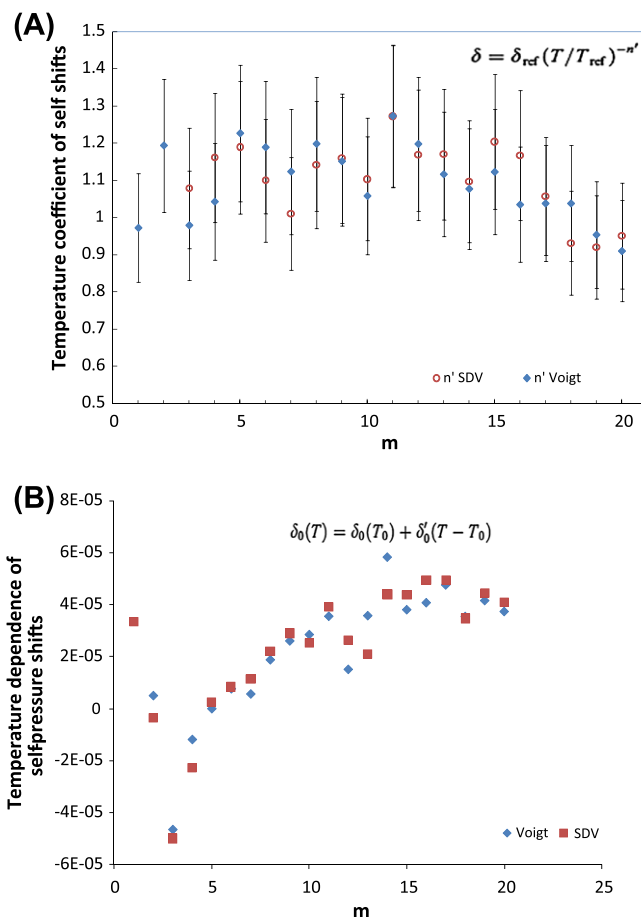
**Fig. 7.** Temperature dependence coefficients for pressure shifts retrieved using the Eqs. (10) (panel A) and (9) (panel B).

Table 6

Temperature dependencies for self broadening coefficients (obtained using Eq. (7)) and pressure induced line self-shift coefficients (obtained using Eqs. (9) and (10)) in the $\nu_1 + \nu_2 + \nu_4 + \nu_5$ band of acetylene.

	n		δ'		n'	
	SDV	Voigt	SDV	Voigt	SDV	Voigt
1	0.60(3)	0.62(3)	0.000033(2)		0.97(5)	
2	0.62(3)	0.63(3)	-0.000004(1)	0.000005(1)	1.19(6)	1.04(5)
3	0.60(3)	0.62(3)	-0.000050(2)	-0.000046(2)	0.98(5)	1.08(5)
4	0.57(3)	0.59(3)	-0.000023(2)	-0.000012(1)	1.04(5)	1.16(6)
5	0.56(3)	0.58(3)	0.000003(1)	-0.000016(1)	1.23(6)	1.19(6)
6	0.59(3)	0.60(3)	0.000008(1)	0.000008(1)	1.19(6)	1.10(5)
7	0.59(3)	0.61(3)	0.000011(1)	0.000006(1)	1.12(6)	1.01(5)
8	0.61(3)	0.63(3)	0.000022(1)	0.000019(1)	1.20(6)	1.14(6)
9	0.60(3)	0.63(3)	0.000029(1)	0.000026(1)	1.15(6)	1.16(6)
10	0.62(3)	0.63(3)	0.000025(1)	0.000028(1)	1.06(5)	1.10(6)
11	0.61(3)	0.63(3)	0.000039(2)	0.000036(2)	1.27(6)	1.27(6)
12	0.58(3)	0.59(3)	0.000026(1)	0.000015(1)	1.20(6)	1.17(6)
13	0.55(3)	0.56(3)	0.000021(1)	0.000016(1)	1.12(6)	1.17(6)
14	0.55(3)	0.56(3)	0.000044(2)	0.000058(3)	1.08(5)	1.10(5)
15	0.55(3)	0.56(3)	0.000044(2)	0.000038(2)	1.12(6)	1.20(6)
16	0.52(3)	0.53(3)	0.000049(2)	0.000041(2)	1.03(5)	1.17(6)
17	0.50(3)	0.51(3)	0.000049(2)	0.000048(2)	1.04(5)	1.06(5)
18	0.51(3)	0.52(3)	0.000035(2)	0.000035(2)	1.04(5)	0.93(5)
19	0.46(2)	0.48(2)	0.000045(2)	0.000042(2)	0.95(5)	0.92(5)
20	0.53(3)	0.54(3)	0.000041(2)	0.000037(2)	0.91(5)	0.95(5)

low m values for both the theoretical and measured coefficients. This behavior seems unphysical and is probably due to the fact that this law is of empirical nature.

3.3. Weak line mixing effects

In this study we found it was necessary to account for weak line mixing effects. The line mixing effects accounting for collisional transfer between pairs of energy levels j and k are modeled by our software by adding an asymmetric profile to the Voigt or speed-dependent Voigt profiles:

$$pY_{ok}(T) = 2p \sum_{j \neq k} \frac{d_j}{d_k} \frac{W_{jk}}{v_k - v_j} \quad (11)$$

Here p is the gas pressure in atm and $Y_{ok}(T)$ is the weak line mixing coefficient of the transition of interest, d_k are the elements of the dipole moment matrix, W_{jk} are off-diagonal elements of the relaxa-

tion matrix that describes the state of the molecule at a given time, v_j are line positions. Note that the self-broadening coefficients are the real parts of the diagonal elements of the relaxation matrix, W , and the pressure-induced line shift coefficients are the imaginary parts of the diagonal elements.

We were able to retrieve experimentally the line mixing coefficients for the spectra recorded at room temperature. But, for consistency in the multispectrum fits at other temperatures, we have modeled the spectral profiles using calculated line mixing coefficients obtained using the Exponential Power Gap scaling law. The calculated and room temperature measured line mixing coefficients are given for the two profiles in Tables 7A and 7B. The errors quoted in the parentheses are estimated from the EPG fits. The calculated sets used in fits with the speed dependent Voigt profile are slightly different than those obtained for the Voigt profile due to the small differences in line broadening and in the intensities retrieved with the two profiles.

We will discuss briefly our Exponential Power Gap calculations for rotational transfer. The off-diagonal elements of the relaxation matrix can be expressed as a function of the collisional transfer rate κ_{jk} as $W_{jk} = -\beta\kappa_{jk}$, where $\beta = 0.56$. We have checked that the sum of the relaxation elements from any column add to zero. The rate of transfer from state k to j must be equal to the rate of transfer from j to k , namely that:

$$\rho_k \kappa_{jk} = \rho_j \kappa_{kj} \quad (12)$$

where ρ_k is the population of the rotational level k . The Exponential Power Gap (EPG) law calculates the collisional transfer rates from the lower rotational level k to a higher rotational level j as,

$$\kappa_{jk} = a(T) \left[\frac{|\Delta E_{jk}|}{B_0} \right]^{-b} \exp \left(\frac{-c|\Delta E_{jk}|}{B_0} \right) \quad (13)$$

where ΔE_{jk} is the energy gap between the two rotational states, B_0 is the rotational constant and a , b , and c are the parameters to be optimized. The line widths have been calculated as,

$$W_{kk} = 1/2 \left[\sum_j \kappa_{jk} \right]_{upper} + 1/2 \left[\sum_j \kappa_{jk} \right]_{lower} \quad (14)$$

We have studied the temperature dependence of the collisional rates and present the empirical fit parameters a , b , c , in Table 8. The parameter a is slowly increasing with temperature, b is nearly

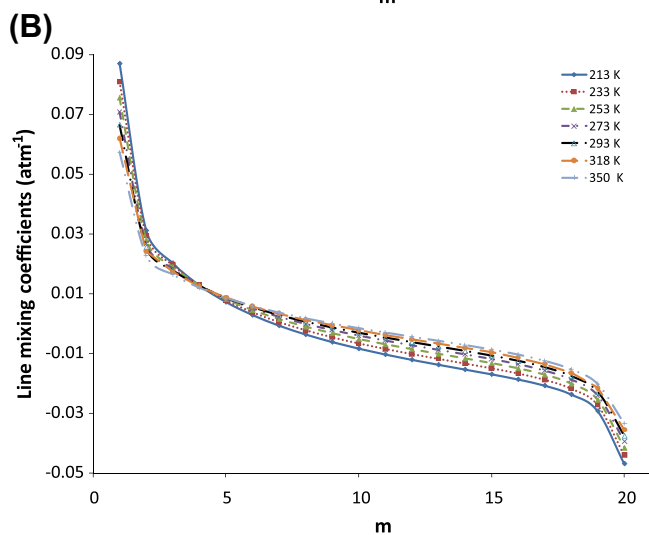
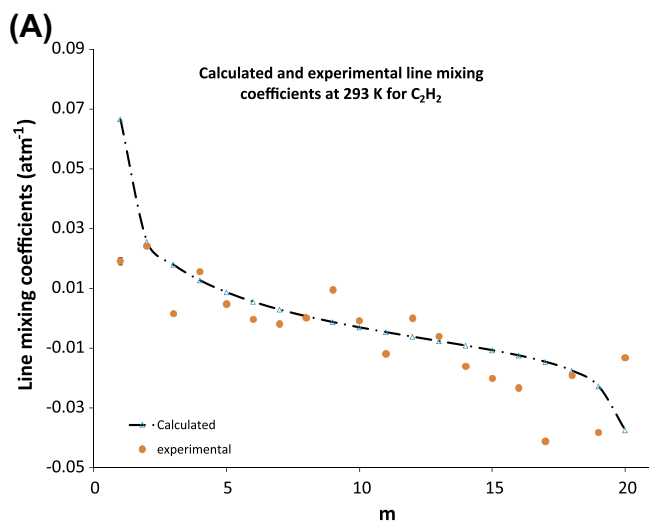
Table 7A

Calculated and measured self-line mixing coefficients in the $\nu_1 + \nu_2 + \nu_4 + \nu_5$ band of acetylene determined using the Voigt profile.

Line	m	213 K	233 K	253 K	273 K	293 K	318 K	350 K	293 K experimental
<i>Self-line mixing coefficients (atm⁻¹) retrieved with the Voigt profile</i>									
R(1)	1	0.0871(124)	0.0809(115)	0.0755(108)	0.0708(101)	0.0665(95)	0.0621(89)	0.0574(82)	0.0191(12)
R(1)	2	0.0313(16)	0.0296(15)	0.0281(14)	0.0268(13)	0.0256(13)	0.0243(12)	0.0229(11)	0.0243(1)
R(2)	3	0.0204(12)	0.0197(12)	0.0191(11)	0.0185(11)	0.0180(11)	0.0173(10)	0.0166(10)	0.0017(4)
R(3)	4	0.0130(6)	0.0130(6)	0.0130(6)	0.0129(6)	0.0128(6)	0.0125(6)	0.0121(6)	0.0157(1)
R(4)	5	0.0074(1)	0.0079(2)	0.0083(2)	0.0086(2)	0.0088(2)	0.0088(2)	0.0088(2)	0.0048(1)
R(5)	6	0.0030(1)	0.0039(1)	0.0046(1)	0.0052(1)	0.0056(1)	0.0059(1)	0.0060(1)	-0.0003(1)
R(6)	7	-0.0005(1)	0.0007(1)	0.0016(1)	0.0024(1)	0.0030(1)	0.0035(1)	0.0038(1)	-0.0018(1)
R(7)	8	-0.0035(1)	-0.0021(1)	-0.0009(1)	0.0001(1)	0.0008(1)	0.0014(1)	0.0019(1)	0.0002(1)
R(8)	9	-0.0060(1)	-0.0044(1)	-0.0031(1)	-0.0021(1)	-0.0012(1)	-0.0005(1)	0.0001(1)	0.0096(3)
R(9)	10	-0.0082(2)	-0.0065(1)	-0.0051(1)	-0.0039(1)	-0.0030(1)	-0.0021(1)	-0.0014(1)	-0.0007(1)
R(10)	11	-0.0102(2)	-0.0083(2)	-0.0068(2)	-0.0056(1)	-0.0046(1)	-0.0037(1)	-0.0029(1)	-0.0119(2)
R(11)	12	-0.0120(3)	-0.0100(3)	-0.0084(2)	-0.0072(2)	-0.0061(2)	-0.0051(1)	-0.0043(1)	0.0001(1)
R(12)	13	-0.0136(2)	-0.0116(2)	-0.0100(2)	-0.0087(2)	-0.0076(1)	-0.0066(1)	-0.0056(1)	-0.0060(1)
R(13)	14	-0.0152(1)	-0.0132(1)	-0.0115(1)	-0.0102(1)	-0.0090(1)	-0.0080(1)	-0.0070(1)	-0.0160(1)
R(14)	15	-0.0168(1)	-0.0148(1)	-0.0131(1)	-0.0117(1)	-0.0106(1)	-0.0095(1)	-0.0085(1)	-0.0201(2)
R(15)	16	-0.0185(4)	-0.0165(3)	-0.0149(3)	-0.0135(3)	-0.0123(3)	-0.0113(2)	-0.0102(2)	-0.0233(2)
R(16)	17	-0.0206(3)	-0.0186(3)	-0.0170(3)	-0.0156(2)	-0.0145(2)	-0.0134(2)	-0.0123(2)	-0.0411(2)
R(17)	18	-0.0235(7)	-0.0216(6)	-0.0200(6)	-0.0186(5)	-0.0174(5)	-0.0163(5)	-0.0152(4)	-0.0191(1)
R(18)	19	-0.0291(2)	-0.0271(2)	-0.0254(2)	-0.0239(2)	-0.0227(2)	-0.0214(2)	-0.0201(2)	-0.0381(4)
R(19)	20	-0.0467(15)	-0.0438(14)	-0.0414(14)	-0.0392(13)	-0.0373(12)	-0.0354(12)	-0.0333(11)	-0.0132(1)

Table 7BCalculated and measured self-line mixing coefficients in the $\nu_1 + \nu_2 + \nu_4 + \nu_5$ band of acetylene determined using the speed dependent Voigt profile.

Line	m	213 K	233 K	253 K	273 K	293 K	318 K	350 K
<i>Self-line mixing coefficients (atm^{-1}) retrieved with the speed-dependent Voigt profile</i>								
R(1)	1	0.0899(136)	0.0833(126)	0.0776(118)	0.0726(110)	0.0682(103)	0.0635(96)	0.0586(89)
R(1)	2	0.0316(18)	0.0298(17)	0.0283(16)	0.0270(15)	0.0258(15)	0.0245(14)	0.0230(13)
R(2)	3	0.0205(13)	0.0199(12)	0.0192(12)	0.0187(11)	0.0181(11)	0.0174(11)	0.0166(10)
R(3)	4	0.0130(6)	0.0131(6)	0.0130(6)	0.0129(6)	0.0128(6)	0.0126(6)	0.0122(6)
R(4)	5	0.0074(2)	0.0080(3)	0.0084(3)	0.0086(3)	0.0088(3)	0.0089(3)	0.0088(3)
R(5)	6	0.0030(1)	0.0039(1)	0.0046(1)	0.0052(1)	0.0056(1)	0.0059(1)	0.0061(1)
R(6)	7	-0.0006(1)	0.0007(1)	0.0016(1)	0.0024(1)	0.0030(1)	0.0035(1)	0.0038(1)
R(7)	8	-0.0036(1)	-0.0021(1)	-0.0009(1)	0.0001(1)	0.0008(1)	0.0014(1)	0.0019(1)
R(8)	9	-0.0061(2)	-0.0045(1)	-0.0032(1)	-0.0021(1)	-0.0012(1)	-0.0005(1)	0.0002(1)
R(9)	10	-0.0084(2)	-0.0066(1)	-0.0051(1)	-0.0039(1)	-0.0030(1)	-0.0021(1)	-0.0014(1)
R(10)	11	-0.0103(2)	-0.0084(2)	-0.0069(1)	-0.0056(1)	-0.0046(1)	-0.0037(1)	-0.0029(1)
R(11)	12	-0.0121(1)	-0.0102(1)	-0.0086(1)	-0.0072(1)	-0.0061(1)	-0.0052(1)	-0.0043(1)
R(12)	13	-0.0138(3)	-0.0118(3)	-0.0101(2)	-0.0088(2)	-0.0076(2)	-0.0066(2)	-0.0057(1)
R(13)	14	-0.0155(1)	-0.0134(1)	-0.0117(1)	-0.0103(1)	-0.0091(1)	-0.0081(1)	-0.0071(1)
R(14)	15	-0.0171(1)	-0.0150(1)	-0.0133(1)	-0.0119(1)	-0.0107(1)	-0.0096(1)	-0.0086(1)
R(15)	16	-0.0189(5)	-0.0168(4)	-0.0151(4)	-0.0137(3)	-0.0125(3)	-0.0114(3)	-0.0104(3)
R(16)	17	-0.0210(3)	-0.0189(2)	-0.0173(2)	-0.0159(2)	-0.0147(2)	-0.0136(2)	-0.0125(2)
R(17)	18	-0.0240(6)	-0.0220(6)	-0.0203(5)	-0.0189(5)	-0.0177(5)	-0.0165(4)	-0.0154(4)
R(18)	19	-0.0297(2)	-0.0276(2)	-0.0258(2)	-0.0243(2)	-0.0230(2)	-0.0217(2)	-0.0203(2)
R(19)	20	-0.0476(14)	-0.0446(13)	-0.042(12)	-0.0398(12)	-0.0379(11)	-0.0358(11)	-0.0336(10)

**Fig. 8.** (A) Overlaid calculated and measured weak self-line mixing coefficients at room temperature. (B) Calculated line mixing coefficients at our set temperatures.

constant and c is slowly decreasing with the increase of temperature.

Table 8

Empirical fit parameters for the Exponential Power Gap scaling law.

Temperature	a	b	c
<i>Voigt model</i>			
213	0.179308(1)	0.410966(1)	0.963011(1)
233	0.165627(1)	0.414418(1)	0.915323(1)
253	0.15372(4)	0.417081(9)	0.865015(4)
273	0.143115(15)	0.418714(12)	0.813391(13)
293	0.133617(1)	0.419518(1)	0.760618(1)
318	0.123812(1)	0.419669(1)	0.707401(1)
350	0.113519(1)	0.418775(1)	0.652258(1)
<i>Speed dependent Voigt model</i>			
213	0.187117(1)	0.420135(1)	0.943237(6)
233	0.172517(1)	0.423451(1)	0.89383(1)
253	0.159819(15)	0.425945(12)	0.841929(13)
273	0.148527(1)	0.427388(1)	0.78882(3)
293	0.138429(1)	0.427986(1)	0.734671(1)
318	0.127995(1)	0.427853(1)	0.679867(1)
350	0.117044(14)	0.42658(17)	0.622872(12)

Fig. 8A shows overlaid measured and calculated line mixing coefficients obtained at room temperature. The variation of calculated line mixing coefficients with temperature can be observed in Fig. 8B. All results are plotted against m . The plotted values correspond only to R-branch transitions and cover the range of our experimental m values. The EPG scaling law modeled the entire range of rotational states, but it doesn't fit perfectly the measured broadening parameters. For $|m|$ values between 4 and 15 the model provides a good agreement with the experimental results.

4. Conclusions

Self broadened line parameters for twenty R-branch transitions in the $\nu_1 + \nu_2 + \nu_4 + \nu_5$ band of acetylene were measured using a 3-channels diode laser spectrometer, a temperature controlled cell of fixed length and a second, room temperature cell. The design allows the users to study the temperature dependence of gases over a wide range of temperatures (195–350 K) and pressures, in different spectral ranges. The performance of the temperature controlled cell is discussed in detail. The pure acetylene profiles have been fitted using Voigt and speed-dependent Voigt profiles, to which we have added dispersion profiles to account for weak line mixing. For each line the spectra recorded at the same temperature were

analyzed using a multispectrum fitting program. The experimental self broadening results were found in good agreement with similar measurements available in the literature. The self-induced broadening coefficients, pressure shifts, line mixing coefficients and their temperature dependences were measured for the first time for transitions in this band.

Acknowledgments

This paper is dedicated to Drs. Bob McKellar and Phil Bunker for their outstanding contributions to the advancement of knowledge in molecular spectroscopy.

A. Predoi-Cross acknowledges financial support from the Natural Sciences and Engineering Research Council of Canada, Canadian Foundation for Innovation and University of Lethbridge Research Funds.

References

- [1] A.A. Madej, A.J. Alcock, A. Czajkowski, J.E. Bernard, Sergei Chepurov, *Journal of the Optical Society of America B* 23 (2006) 2200–2208.
- [2] A. Coustenis, R.K. Achterberg, B.J. Conrath, D.E. Jennings, A. Marten, D. Gautier, C.A. Nixon, F.M. Flasar, N.A. Teanby, B. Bezard, R.E. Samuelson, R.C. Carlson, E. Lellouch, G.L. Bjoraker, P.N. Romani, F.W. Taylor, P.G.J. Irwin, T. Fouchet, A. Hubert, G.S. Orton, V.G. Kunde, S. Vinatier, J. Mondellini, M.M. Abbas, R. Courtin, *Icarus* 189 (2007) 35–62.
- [3] P. Varanasi, R.P. Bangaru, *Journal of Quantitative Spectroscopy & Radiative Transfer* 15 (1975) 267–273.
- [4] J.S. Wong, *Journal of Molecular Spectroscopy* 82 (1980) 449–451.
- [5] D. Lambot, A. Olivier, J. Walrand, G. Blanquet, J.P. Bouanich, *Journal of Quantitative Spectroscopy & Radiative Transfer* 45 (1991) 145–155.
- [6] A.S. Pine, *Journal of Quantitative Spectroscopy & Radiative Transfer* 50 (1993) 149–166.
- [7] D. Lambot, J.C. Populaire, J. Walrand, G. Blanquet, J.P. Bouanich, *Journal of Molecular Spectroscopy* 165 (1994) 1–11.
- [8] A. Lucchesini, M. DeRosa, D. Pelliccia, A. Ciucci, C. Gabbanini, S. Gozzini, *Applied Physics B – Lasers and Optics* 63 (1996) 277–282.
- [9] R. Georges, D. Van Der Vorst, M. Herman, D. Hurtmans, *Journal of Molecular Spectroscopy* 185 (1997) 187–188.
- [10] D. Biswas, B. Ray, S. Dutta, P.N. Ghosh, *Applied Physics B – Lasers and Optics* 68 (1999) 1125–1130.
- [11] F. Herregodts, D. Hurtmans, J. Vander Auwera, M. Herman, *Journal of Chemical Physics* 111 (1999) 7954–7960.
- [12] C. Yelleswarapu, A. Sharma, *Journal of Quantitative Spectroscopy & Radiative Transfer* 69 (2001) 151–158.
- [13] P. Minutolo, C. Corsi, F. D'Amato, M. De Rosa, *European Physical Journal D* 17 (2001) 175–179.
- [14] H. Valipour, D. Zimmerman, *Journal of Chemical Physics* 114 (2001) 3535–3545.
- [15] D. Jacquemart, J.Y. Mandin, V. Dana, L. Regalia-Jarlot, X. Thomas, P. Van der Heyden, *Journal of Quantitative Spectroscopy & Radiative Transfer* 75 (2002) 397–422.
- [16] M. Lepere, G. Blanquet, J. Walrand, J.P. Bouanich, M. Herman, J.V. Auwera, *Journal of Molecular Spectroscopy* 242 (2007) 25–30.
- [17] D. Jacquemart, O.M. Lyulin, N. Lacombe, V.I. Perevalov, J.-Y. Mandin, *Journal of Quantitative Spectroscopy & Radiative Transfer* 109 (2008) 1856–1874.
- [18] J.S. Li, G. Durry, J. Cousin, L. Joly, B. Parvitte, V. Zeninari, *Journal of Quantitative Spectroscopy & Radiative Transfer* 111 (2010) 2332–2340.
- [19] D. Mondelain, C. Camy-Peyret, A.W. Mantz, E. Tang, A. Valentin, *Journal of Molecular Spectroscopy* 241 (2007) 18–25.
- [20] Z. El Helou, B. Erba, S. Churassy, G. Wannous, M. Neri, R. Bacis, E. Boursey, *Journal of Quantitative Spectroscopy & Radiative Transfer* 101 (2006) 119–128.
- [21] R.E. Shetter, J.A. Davidson, C.A. Cantrell, J.G. Calvert, *Review of Scientific Instruments* 58 (1987) 1427–1428.
- [22] A.R.W. McKellar, *Faraday Discussions* 97 (1994) 69–80.
- [23] A.R.W. McKellar, J.K.G. Watson, B.J. Howard, *Molecular Physics* 86 (1995) 273–286.
- [24] J. Ballard, K. Strong, J.J. Remedios, M. Page, W.B. Johnston, *Journal of Quantitative Spectroscopy & Radiative Transfer* 52 (1994) 677–691.
- [25] K. Strong, F.W. Taylor, S.B. Calcutt, J.J. Remedios, J. Ballard, *Journal of Quantitative Spectroscopy & Radiative Transfer* 50 (1993) 363–429.
- [26] D. Newnham, J. Ballard, M. Page, *Review of Scientific Instruments* 66 (1995) 4475–4481.
- [27] K.M. Smith, D.A. Newnham, *Journal of Geophysical Research – Atmospheres* 105 (2000) 7383–7396.
- [28] R.A. McPheat, D.A. Newnham, R.G. Williams, J. Ballard, *Applied Optics* 40 (2001) 6581–6586.
- [29] Y. Abebe, C.D. Ball, F.C. De Lucia, A.W. Mantz, *Spectrochimica Acta Part A – Molecular and Biomolecular Spectroscopy* 55 (1999) 1957–1966.
- [30] A. Valentin, A. Henry, C. Claveau, C. Camy-Peyret, D. Hurtmans, A.W. Mantz, *Spectrochimica Acta Part A – Molecular and Biomolecular Spectroscopy* 60 (2004) 3477–3482.
- [31] M.A.H. Smith, C.P. Rinsland, V.M. Devi, D.C. Benner, *Spectrochimica Acta Part A – Molecular and Biomolecular Spectroscopy* 48 (1992) 1257–1272.
- [32] M.W.P. Cann, *Review of Scientific Instruments* 40 (1969) 595–607.
- [33] R.D. Schaeffer, J.C. Sproul, J. Oconnell, C. Vanvloten, A.W. Mantz, *Applied Optics* 28 (1989) 1710–1713.
- [34] A. Predoi-Cross, C. Hnatovsky, K. Strong, J.R. Drummond, D.C. Benner, *Journal of Molecular Structure* 695 (2004) 269–286.
- [35] V.S.I. Sprakel, M.C. Feiters, R.J.M. Nolte, P.M.F.M. Hombergen, A. Groenen, H.J.R. De Haas, *Review of Scientific Instruments* 73 (2002) 2994–2998.
- [36] D. Hurtmans, G. Dufour, W. Bell, A. Henry, A. Valentin, C. Camy-Peyret, *Journal of Molecular Spectroscopy* 215 (2002) 128–133.
- [37] L.S. Rothman, I.E. Gordon, A. Barbe, D. Chris Benner, P.F. Bernath, M. Birk, V. Boudon, L.R. Brown, A. Campargue, J.-P. Champion, K. Chance, L.H. Coudert, V. Dana, V.M. Devi, S. Fally, J.-M. Flaud, R.R. Gamache, A. Goldman, D. Jacquemart, I. Kleiner, N. Lacombe, W.J. Lafferty, J.-Y. Mandin, S.T. Massie, S. Mikhailenko, C.E. Miller, N. Moazzen-Ahmadi, O.V. Naumenko, A. Nikitin, J. Orphal, A. Predoi-Cross, V. Perevalov, A. Perrin, C.P. Rinsland, M. Rotger, M. Šimečková, M.A.H. Smith, K. Sung, S. Tashkun, J. Tennyson, R.A. Toth, A.C. Vandaele, J. Vander Auwera, *Journal of Quantitative Spectroscopy and Radiative Transfer* 110 (9–10) (2009) 533–572.
- [38] M. Herman, *Molecular Physics* 105 (17–18) (2009) 2217–2241.